Automatika

Journal for Control, Measurement, Electronics, Computing and Communications

ISSN: (Print) (Online) Journal homepage: https://www.tandfonline.com/loi/taut20

Hybrid power generation forecasting using CNN based BILSTM method for renewable energy systems

T. Anu Shalini & B. Sri Revathi

To cite this article: T. Anu Shalini & B. Sri Revathi (2023) Hybrid power generation forecasting using CNN based BILSTM method for renewable energy systems, Automatika, 64:1, 127-144, DOI: 10.1080/00051144.2022.2118101

To link to this article: https://doi.org/10.1080/00051144.2022.2118101

Published online: 05 Sep 2022.

AUTOMATIKA
2023, VOL. 64, NO. 1, 127–144
https://doi.org/10.1080/00051144.2022.2118101

REGULAR PAPER

OPEN ACCESS Check for updates

Hybrid power generation forecasting using CNN based BILSTM method for renewable energy systems

T. Anu Shalini and B. Sri Revathi

School of Electrical Engineering, Vellore Institute of Technology, Chennai, India

ABSTRACT

This paper presents the design of a grid-connected hybrid system using modified Z source converter, bidirectional converter and battery storage system. The input sources for the proposed system are fed from solar and wind power systems. A modified high gain switched Z source converter is designed for supplying constant DC power to the DC-link of the inverter. A hybrid deep learning (HDL) algorithm (CNN-BiLSTM) is proposed for predicting the output power from the hybrid systems. The HDL method and the PI controller generate pulses to the proposed system. A closed loop control framework is implemented for the proposed grid integrated hybrid system. A 1.5 Kw hybrid system is designed in MATLAB/SIMULINK software and the results are validated. A prototype of the proposed system is developed in the laboratory and experimental results are obtained from it. From the simulation and experimental results, it is observed that the ANN controller with SVPWM (Space vector Pulse width Modulation) gives a THD (Total harmonic distortion) of 2.2% which is within the IEEE 519 standard. Therefore, from the results, it is identified that the ANN-SVPWM method injects less harmonic currents into the grid than the other two controllers.

ARTICLE HISTORY
Received 14 November 2021
Accepted 23 August 2022

KEYWORDS
Artificial Neural Network; convolutional neural network; bidirectional long short time memory neural network

1. Introduction

The world's population growth is increasing exponentially and so is the energy requirement. Conventional energy sources like fossil-fuel-based generators, nuclear power plants and hydropower plants have served us good so far, but create environmental pollution and climatic changes [1]. With green-house emissions from the thermal power plants there has been a considerable climatic change. In addition, the fossil-fuels are being depleted at an alarming rate. Hence, initiatives are being taken up by various firms to replace the conventional energy sources with green energy sources like solar and wind. The extraction of energy from the renewable energy sources cannot be precisely planned, as these sources are weather dependent. Solar energy generation [2] is dependent on irradiance, temperature, wind speed and cloud cover; whereas wind energy [3] generation is dependent on wind speed, temperature, pressure and humidity. This causes high variability and seasonal deviations in energy generation; moreover, it does not follow the load demand profile. Thus, the integration of large amounts of solar and wind generators in the power grids can lead to lowered reliability and stability.

In order to increase the penetration of renewable energy systems into the conventional power grid, forecasts at multiple time horizons can play an important role. A good forecasts [4] can make effective planning of renewable energy generation. Also, highly accurate forecasts can help in grid regulation, power scheduling, unit commitment and load-following. Numerous experts throughout the world are currently conducting detailed study on solar [5] and wind energy [6] prediction methods. Solar and Wind power prediction techniques can be classified into three broad categories based on their prediction concepts: physical approach, statistical approach and machine learning approach [7]. Machine learning (ML) has experienced significant growth in prediction applications as artificial intelligence has progressed. Higher accuracy and a more perfect extraction of renewable power is obtained by the machine learning strategy during the change in output curve of solar and wind power significantly. ANN (Artificial Neural Network) with back propagation can be used successfully for wind speed forecasts, and similar ANN models can be used for forecasting other weather variables like Dew-Point Temperature, Relative Humidity, Wind Direction and Pressure [8]. ANN and NWP (Numerical Weather Prediction) are the best model choices for wind speed prediction [9]. ARIMA (Autoregressive Integrated Moving Average), ANN and NWP methods are a good choice for short-term (intra-hour and intra-day) and long-term (day-ahead; NWP) forecasting. Although some

CONTACT B. Sri Revathi srirevathi.b@vit.ac.in School of Electrical Engineering, Vellore Institute of Technology, Chennai Campus, Chennai, India

updated machine learning approaches have reached excellent reliability and efficiency, they continue to face challenges when processing vast amounts of input data and interacting with disappearing or bursting gradients. As a result, the DL technique [10] has been applied in the forecasting process in order to address the drawbacks of ML methods. There are several deep learning methods used in forecasting the renewable power. They are convolutional neural network [11] (CNN), generative adversarial networks [12] (GAN), deep belief network [13] (DBN), bidirectional long short time memory neural network [14] (Bi-LSTM) and deep residual learning [15] (DRL). The CNN method is used in several load and solar irradiation forecasting applications and has not been used for wind power applications. The sparse connectivity and parameter sharing properties of CNN makes it to use fewer training variables, reduces the time in training process and enhances the forecasting efficiency. In the first stages of its development, the CNN model is designed for image processing, which is better suited for analyzing two-dimensional information. The use of CNN increases the complexity and decreases the accuracy as information is translated from one-dimensional to two-dimensional form. Therefore, the LSTM model [16] is mostly preferred in tackling time series problems due to its ability to analyze sequential data. The LSTMs include particular loops that allow data to persist for longer. In this variant of ANN, the input parameters are not processed twice, but instead they are just cross-referenced once (from the input). The prediction is computed based on previous and real-time data from the network to the output. The use of hybrid forecasting models can improve the accuracy of the forecasting system [17]. The authors in [18] proposed the hybrid DL method (CNN-GRU) which can effectively predict the very short-term wind generation in Australia. The CNN-GRU method is compared with other existing methods and the proposed method performs well for wind farms. In [19] the authors used the CNN-GRU with HHO method for forecasting the wind power in the Boco Rock Wind Farm in Australia. The suggested hybrid DL method obtained an accuracy of 38% and 24% during prediction for 5–10 min. The authors in [20] proposed the CNN + LSTM approach for predicting the photovoltaic output power. Experimental investigations were done using the real-time data and the test results proved that the CNN + LSTM approach provides accurate forecasting than other DL methods. A Higher-order multivariate Markov chain (HMMC) method is implemented for the prediction of solar and wind power in [21]. The proposed method considers the heat index for forecasting the output power accurately. From the results, the proposed method performs well in terms of accuracy. The authors in [22–24] discussed the implementation of HDL methods in hybrid power generation forcasting. From the literature it is observed that most of the work are carried out using the CNN and other DL method. The important advantage of using CNN is that it automatically detects the filters for feature identification on its own. When the CNN is trained with the solar and wind data, the CNN uses the backpropagation algorithm and will find out the right amount of filter used for feature extraction. The training of any neural network is a repetitive process in which some variant of gradient descent is used. In a neural network, the necessity of the gradient is to indicate, how to alter the variables, in order to reduce the model's error. But in deep learning methods this gradient is unstable. Therefore, when the Recurrent Neural Networks (RNN) are trained, the gradient is calculated not only through various layers but also through time. Vanilla RNN contains a restriction that both input and output must be of the same size. The long short-term memory type of RNN is superior to other RNNs since it can overcome the vanishing or exploding gradient descent problem. Another type of RNN is the bidirectional long short-term memory (BILSTM) is developed with the goal of increasing the prediction performance, and permits two sets of training stages during which the input parameters are used in both directions (backward and forward). The BiLSTMs models are derived from the accumulation of prior and forthcoming step input data (i.e. information that pertains to past and future time steps) to a specific time step in LSTM models. As a result, in BiLSTMs, past and future information are retained at any moment in time. Therefore, in the proposed work the BILSTM type RNN is used, where the real-time data available on solar and wind along with the previous data of solar and wind are used for accurate prediction of output power. The problems in implementing the forecasting methods for the wind and solar power system can be described as follows:

- Wind and Solar energy's inevitable intermittent nature and variability makes inaccurate prediction of wind and solar power generation.
- Few studies have examined the bidirectional learning capability of Bi-LSTM in the context of wind and solar energy prediction, while the majority of research has concentrated on LSTM.
- From the literature it has been identified that, the hybrid deep learning method (CNN-BiLSTM) has not yet been used for prediction of hybrid power generation.
- There has been no standardized assessment and validation of several deep learning techniques (CNN, LSTM, Bi-LSTM, CNN-Bi-LSTM) in the wind and solar energy forecasting domain.

Finally, to address the constraints and fill in the limitations mentioned above,

- A HDL method (CNN-BiLSTM) is presented in this article to estimate the short-term solar and wind power output by effectively reaping the benefits of the bilateral temporal pattern extraction of Bi-LSTM and spatial pattern extraction ability of CNN.
- A modified switched Z-source converter is implemented in the proposed system
- In solar and wind energy prediction, model comparisons between various DL models (CNN, BiLSTM, CNN-BiLSTM) are conducted.

The following summarizes the hierarchy of the article. The first section explains the paper's topic and challenge through a literature study and outlines the existing gaps and challenges in the field of wind and solar energy forecasting; The second section details the modular switched Z source converter and design of the various components in the proposed system. The third section discusses how to apply the CNN-BiLSTM approach to solar and wind energy systems. The fourth section discusses the proposed system's control; The final section discusses the suggested system's results and conclusions.

2. Proposed system

The hybrid renewable energy configuration, including the converter and the control system, is depicted in Figure 1. In order to facilitate better energy output from the DC sources and to integrate the DC sources with the grid, PV panels, a wind energy conversion system and a storage battery are used in the proposed system. There is a converter unit to regulate the output power from the DC sources and an inverter unit to integrate with the grid. The photovoltaic system is made up of a collection of photovoltaic panels which are interconnected in order to harvest the maximum amount of energy possible. It is necessary to implement a switched Z-Source converter in order to boost the array voltage to a level that is equivalent to the DC voltage at the Point of Common Coupling (PCC). The wind energy system is comprised of wind turbines, a turbo generator and a diode bridge rectifier, boost converter, which regulates the amount of wind energy produced. If there is zero power generation from solar and wind power, a chain of batteries is installed to maintain a constant voltage at the PCC and inject the power into the grid. PI controller controls the charging and discharging modes of the battery bank in the secondary storage system. The secondary storage system also includes a bidirectional converter. This converter is utilized as an intermediate between the storage device and the PCC, and it regulates the current flow when the line voltage at the PCC and the storage device are varied.

The grid coordinated inverter converts the direct current (DC) power produced by the hybrid renewable sources into alternating current and feeds it back into the grid. When combined with an inverter and battery, a feedback controller (PI controller) is used to regulate the hybrid energy system, resulting in a hybrid power monitoring and control system that is both reliable and efficient in operation. When it comes to controlling the power flow, the centralized power management system is comprised of ANN that is facilitated by artificial intelligence to integrate both the transient and steady-state power flow.

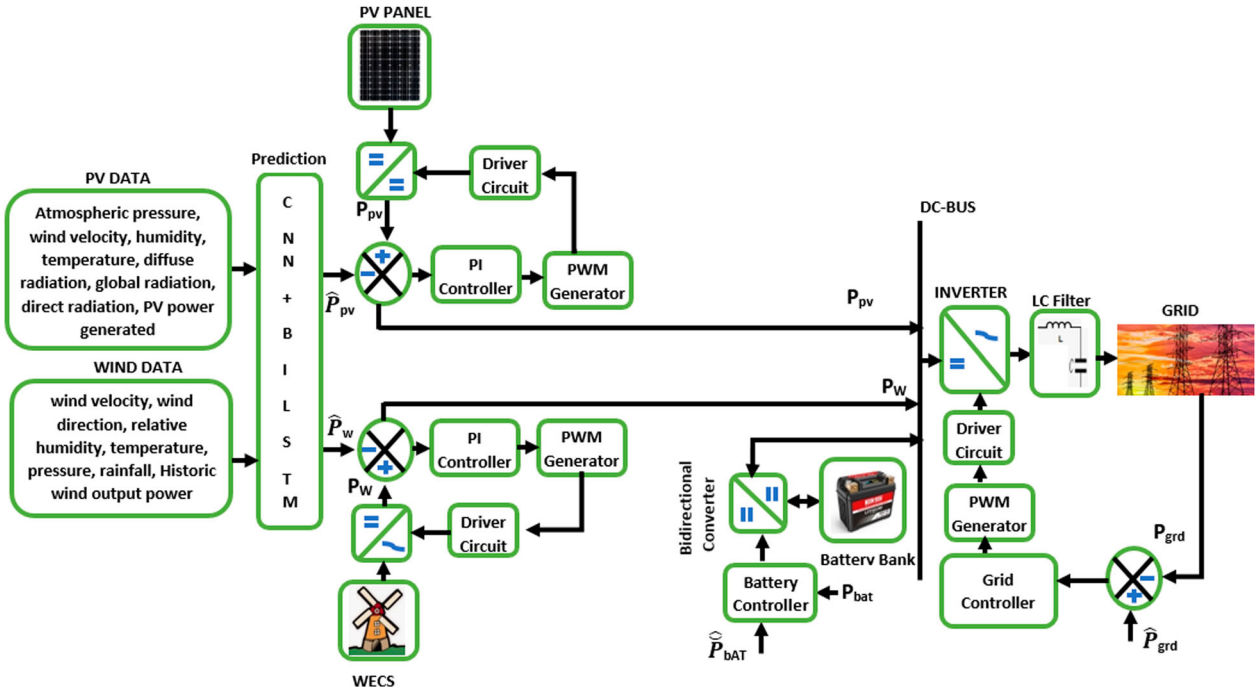

Figure 1. Block diagram of the proposed system.

2.1. Proposed modified switched Z-source converter (MSZSC)

The proposed converter is designed by considering the basic topology of the Z-source converter circuit. The input to the proposed converter is fed from PV panels. Figure 2 presents the basic structure of the PV panel. In the modified converter a slight modification is done in the circuit by incorporating a capacitor C_2 and a diode D_2 to the other circuitry elements C_1 and D_1. Therefore, a switched capacitor circuit has been developed by using the components C_1, C_2 and D_1, D_2. To achieve a higher voltage gain, the suggested converter maintains constant current flow. To understand the static characteristics of the converter the storage elements are assumed to be ideal and equal in nature.

Figure 3 presents the modified Z source circuit with its operating modes. These modes are also known as stages and operate by turning on and off the semiconductor switch S.

2.1.1. Mode I

During the conduction of switch S, the semiconductor diodes D_1, D_2 open due to their anti-parallel connection with the capacitor. V_i and C_3 makes the inductor L_1 to charge, and V_i and C_2 makes the inductor L_2 to charge. Since V_i, C_1, and C_2 are connected in a sequence, the DC power is supplied to the load through the switch S. The underlying steady-state equations are derived using KVL to the circuit presented in Figure 3(b).

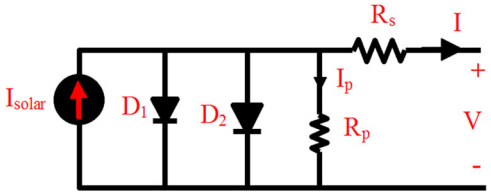

Figure 2. PV cell basic structure.

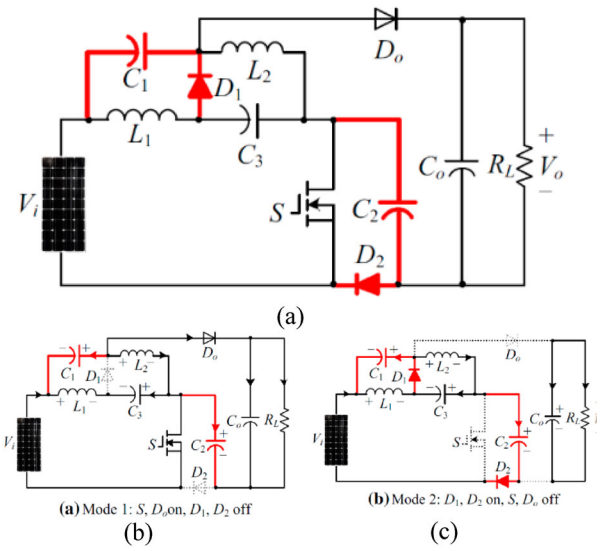

Figure 3. (a) Switched Z-source converter (b) Mode I (c) Mode II.

$$V_{L1} = V_i + V_{C3} \tag{1}$$

$$V_{L2} = V_i + V_{C1} \tag{2}$$

$$V_0 = V_i + V_{C1} + V_{C2} \tag{3}$$

When the switch S is in off condition, the diodes D_1, D_2 starts conducting. Since the output diode D_o is in reverse blocking state, the capacitances C_1, and C_3 gets charged through the inductors L_1 and L_2. Since the inductor L_1 is in series with inductor L_2, the capacitor C_2 charges through the input voltage source V_i and the inductor L_1. Therefore current in the converter circuit flows through the output capacitor C_o to the RL load. The underlying steady-state equations are derived using KVL to the same circuit presented in Figure 3(b) with switch S in closed position.

$$V_{L1} + V_{C1} = 0 \tag{4}$$

$$V_{L2} + V_{C3} = 0 \tag{5}$$

$$V_i = V_{L1} - V_{C3} + V_{C2} \tag{6}$$

Under stable conditions the voltage across the inductor is equal to zero.

Therefore

$$V_{C1} = V_{C3} = \frac{D}{1-2D} V_i \tag{7}$$

$$V_{C2} = V_i + V_{C1} + V_{C3} = \frac{1}{1-2D} V_i \tag{8}$$

From Equations (11), (12) the output voltage V_0 is presented in Equation (13).

$$V_0 = V_i + V_{C1} + V_{C2} = \frac{2-D}{1-2D} V_i \tag{9}$$

The gain (G) of the proposed modified converter is:

$$G = \frac{V_0}{V_i} = \frac{2-D}{1-2D} \tag{10}$$

2.2. Modelling of bidirectional converter

Bidirectional converters and battery units are used to ensure the electrical potential at PCC as high as possible, which exceeds the threshold storage capacity of batteries (540 V). Single-cell batteries must use voltage equalization circuitry to ensure that all cells deliver the same voltage. To achieve voltage equalization a battery of low voltage rating is connected in series with the battery packs. Therefore, the optimal dc link voltage is maintained stable at the PCC which improves the battery life cycle. In the beginning, the conduction time for the switching pulses is kept at 50%, and the converter does not operate in either step-up or step-down

mode, and there is no power flow among both the battery and grid. The difference between the magnitude of the PCC voltage and the terminal voltage level of the battery packs, alters the operational sequence of the converter controlled by the PI controller [25].

When the renewable energy output falls below the battery voltage, the bidirectional converter boosts the power from the battery packs to the PCC. When the PCC voltage falls below the battery voltage, the bidirectional converter makes the battery packs to charge since power begins to flow from the PCC to the battery. A battery is also installed at the PCC to reduce the level of stress and to maintain a constant power supply. It is important to adhere to the state of charge (SOC) of the batteries in order to assure appropriate planning. SOC provides information regarding the thermal resistance, internal resistance, temperature, present charge and ageing of battery. In the majority of the implementations, actual contribution on ampere-hour calculation is used to measure SOC.

$$\mathrm{SOC}(t) = \mathrm{SOC}(0) - \frac{1}{Q}\int_0^t I(t)dt \qquad (11)$$

It is absolutely critical to keep the SOC (or "state of charge") of the battery within the base as high as possible in order to utilize battery energy efficiently and hence earn electricity for use. The battery usage limits suggested are set between 20% and 90% of SOC (Figure 4).

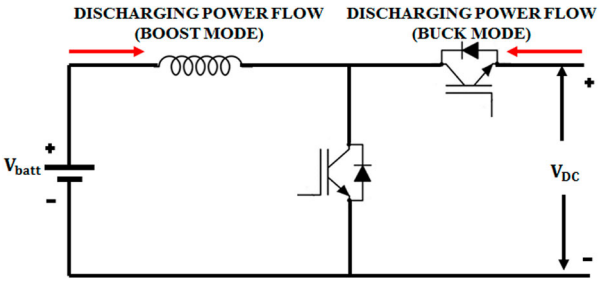

Figure 4. Bidirectional Power flow in Battery setup.

3. Methodology

In general, a Neural network is used to handle the variety of inputs such that it can classify the variety of inputs in a generic way. The use of ANN in image classification is less efficient since it requires more computations. Image identification task is highly centred around the locality of the image. The ANNs cannot differentiate the local pixel and far pixel in an image. Moreover, the ANNs are hypersensitive to the region of an object in the image. Considering the disadvantages of ANNs the hybrid deep learning methods are proposed. The hybrid deep learning method used in the proposed work is CNN-BiLSTM. The major objective of this work is to make accurate and robust forecasting in hybrid power generation systems. For accurate forecasting, the present and past data of solar and wind energy systems are mandatory. It is essential to pre-process and evaluate the data before feeding the data to the model. Therefore, the pre-processing reduces the complexity and increases the efficiency of the prediction models. Before processing, all the abnormal data are eliminated and the missing data are filled. Thus, the data are normalized. The advantages of the BiLSTM and CNN are discussed in the literature. While CNN is superior at mapping constant spatial properties of data, BI-LSTM can recognize long-term temporal connections in bidirectional ways. Thus, in order to better anticipate the short-term solar and wind power output, a hybrid model consisting of CNN and Bi-LSTM is presented. Figure 5 presents the block diagram of the hybrid DL model.

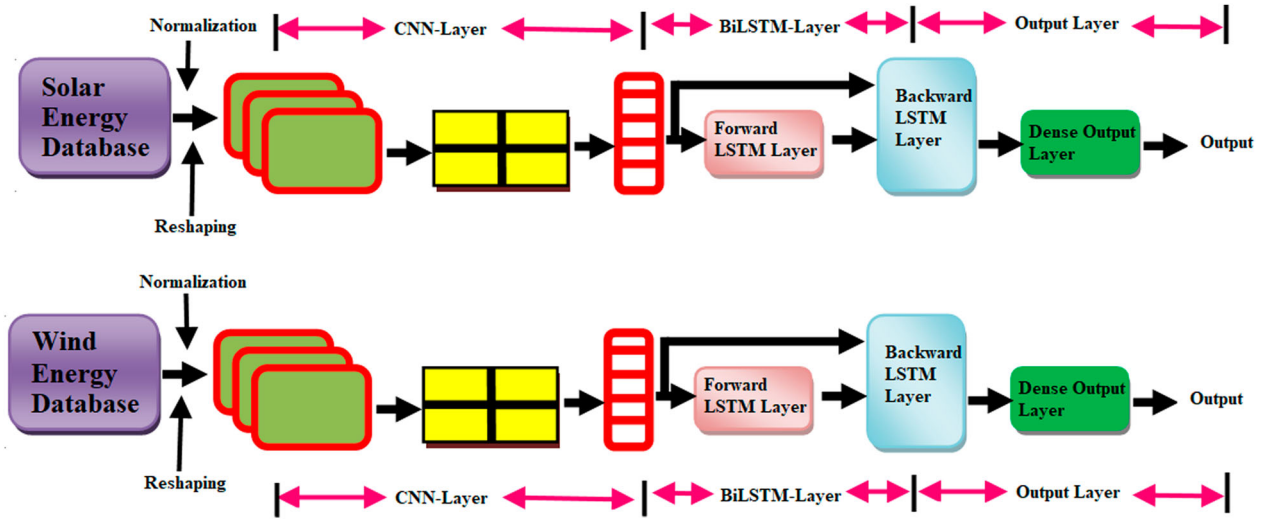

Figure 5. Block diagram of the proposed DL model.

3.1. Convolution neural network (CNN)

CNN collects the model parameters from the incoming solar and wind database as presented in Figure 5. The CNN model is built with a convolution layer, max-pooling layer and flattening layer. In CNN two process takes place, one is the feature extraction and the other is the classification. In the first process, the convolution layer and ReLU are present. Convolution layer is used to process the solar and wind database that comes in as input. By doing a convolution operation, a feature map is created to identify the particular feature. The ReLU activation is used to bring the nonlinearity in the model. The activation function (ReLU) is employed in the CNN layer to conduct elementwise computations. The role of the ReLU is to explore a feature map, and replace the negative values with zeros. ReLU fastens the training and computations. After the convolution layer there is another layer called pooling layer. This layer is used to reduce the size or dimensions of the feature. The new feature generated after the pooling layer will be half the size of the previously extracted feature obtained from the convolution layer. There are two types of pooling namely max and average pooling. Max pooling along with convolution gives a position invariant feature detection. Since max pooling uses less parameters in the process of feature extraction, overfitting is reduced. Max pooling layer is also resistant towards disturbances and variations. The net output obtained from the convolution and the Max Pooling layer is fed to the classification process. In this stage, the obtained output is fed to a densely connected neural network. Therefore, the required output can be obtained from the CNN. By applying this learning algorithm, the gradient difficulties such as gradient vanishing and gradient explosion in RNN can be avoided. In the convoluted output, the feature vectors of larger values are extracted.

3.2. Bidirectional long short-term memory (BILSTM)

Different categories of RNNs possess different structures; they can learn next states solely from previous states. However, the complete training dataset from the input is required for the time series prediction. In order to deal with the issue of time series data, bidirectional RNNs have been created. Both the previous and present values can be fed into BiLSTM layer, which, however, assigns greater weight to the existing situation at time t to forecast the future state. Time-series prediction on the BiLSTM layer begins with the output from the flattering layer. To deal with the gradient diminishing problem of RNNs, the BiLSTM uses an update and relevance gate. The influence of these gates affects the present state output at time t. This is the process that is used to predict the output power of solar and wind using the solar and wind parameters.

3.2.1. Steps involved in predicting the solar and wind power using CNN-BiLSTM

Stage1 – Collecting the solar and wind data presented in Figure 1 from the geographical location.

$$\mathrm{PV} = \{\mathrm{PV}_{1,1}, \mathrm{PV}_{1,2}, \mathrm{PV}_{1,3}, \ldots, \mathrm{PV}_{1,\mathrm{T}}\},$$
$$\mathrm{WP} = \{\mathrm{WP}_{1,1}, \mathrm{WP}_{1,2}, \mathrm{WP}_{1,3}, \ldots, \mathrm{WP}_{1,\mathrm{T}}\},$$

Stage2 – The data collected for the deep learning model is validated from 0 to1.

Stage3 – The homogenized data are transformed into a 3-dimensional matrix structure. The data validation will verify that information is on similar scale.

Stage4 – The homogenized set of data is immediately transmitted into the single-dimensional convolution layer having a filtration system with size $\boldsymbol{Sz}$. Therefore, the weight at time $\boldsymbol{t}$ is determined by

$$\boldsymbol{W_{pv(t)} = F_k^{Sz-1} * F_k^{Sz} * n_c^{Sz-1} * n_c^{Sz}},$$
$$\boldsymbol{W_{Wp(t)} = F_k^{Sz-1} * F_k^{Sz} * n_c^{Sz-1} * n_c^{Sz}} \quad (12)$$

and bias is determined as $\boldsymbol{B_t^k = n_c^{Sz}}$.

The output of the single-dimensional convolutional layer for predicting the solar output power is determined by

$$\boldsymbol{C(t) = W_{pv(t-1)} * A_{pv(t-1)} + B_t^k} \quad (13)$$

The output of the single-dimensional convolutional layer for predicting the wind output power is determined by

$$\boldsymbol{C(t) = W_{wp(t-1)} * A_{wp(t-1)} + B_t^k} \quad (14)$$

where $\boldsymbol{A_{pv(t-1)}, A_{wp(t-1)}}$ is the activation function of the solar system and the activation function of the wind system.

$$\boldsymbol{A_{pv(t)} = A_{wp(t)} = G(C(t))} \quad (15)$$

where $\boldsymbol{G(c(t))}$ represents the nonlinearity in activation function corresponding to time $\boldsymbol{t}$.

The parameters obtained from the convolution layer are fed as the input to the max pooling layer in which the feature extraction is done under moderate dimensions.

$$\boldsymbol{Mx_H * Mx_W * n_c} = \left(\frac{\boldsymbol{Mx_H - F}}{\boldsymbol{PV}} + 1\right) * \left(\frac{\boldsymbol{Mx_W - F}}{\boldsymbol{PV}} + 1\right) \quad (16)$$

$$\boldsymbol{Mx_H * Mx_W * n_c} = \left(\frac{\boldsymbol{Mx_H - F}}{\boldsymbol{WP}} + 1\right) * \left(\frac{\boldsymbol{Mx_W - F}}{\boldsymbol{WP}} + 1\right) \quad (17)$$

where $\boldsymbol{Mx_H, Mx_W}$ represent the height and width of matrix.

Stage5 – The information to the BiLSTM layer is generated by the max-pooling layer. Currently stored memory content at time t is the value of the most recently active cell and the preceding information, as well as a bias. The foreget gate memory device, known as a memory cell unit GM(t), retains the data about the past and present state. The input gate gets the value for the input from the previous CNNs max-pooling layer. The memory control also determines what information should be held in the memory module.

$$\boldsymbol{P_t} = \boldsymbol{\sigma}(\boldsymbol{W_i}[\boldsymbol{GM_{t-1}}, \boldsymbol{X_t}] + \boldsymbol{B_t^k}) \tag{18}$$

The forget gate GM is responsible for deciding the past state data to eliminate.

$$\boldsymbol{GM_t} = \boldsymbol{\sigma}(\boldsymbol{W_f}[\boldsymbol{GM_{t-1}}, \boldsymbol{X_t}] + \boldsymbol{B_t^k}) \tag{19}$$

Non-linearity is added to the system with the ***tanh*** nonlinear activation factor in the ***tanh*** activation stack.

$$\boldsymbol{C'(t)} = \boldsymbol{tanh}(\boldsymbol{W_c}[\boldsymbol{GM_{t-1}}, \boldsymbol{X_t}] + \boldsymbol{B_t^k}) \tag{20}$$

When the input state is same, the memory cell retains the data and when the input state is different, the forget gate removes the data.

$$\boldsymbol{C(t)} = \boldsymbol{GM_{t-1}} * \boldsymbol{C_{t-1}} + \boldsymbol{P_t} * \boldsymbol{C'(t)} \tag{21}$$

An output gate determines which layer state should be the output.

$$\boldsymbol{A_{(t)}} = \boldsymbol{\sigma}(\boldsymbol{W_o}[\boldsymbol{GM_{t-1}}, \boldsymbol{X_t}] + \boldsymbol{B_t^k}) \tag{22}$$

BiLSTM accepts the data from both left and right gates. This differs from LSTM, which only takes information from the preceding gate.

$$\boldsymbol{h_{(t)BiLSTM}} = \boldsymbol{h_{(t)forward}} * \boldsymbol{h_{(t)backward}} \tag{23}$$

For detailed assessment, the suggested hybrid DL model is validated with a variety of DL models on a variety of performance parameters. Investigation has been done with common parameters such as mean square error (MSE), mean absolute error (MAE) and r^2 error in this work. Furthermore, distribution errors like skewness and kurtosis errors are also considered.

4. Control system of the proposed system

The proposed system uses PI controller for the PV system, Wind energy conversion system and Bidirectional converter. Parametric tuning of PI controller can be seen as one of the most critical engineering tasks during control system authorizing to obtain the preferences for control responses. Parametric PI Controller [26] tuning is a compromise between reaction speed and small-signal disturbance stability and tolerance to major signal disturbances. Initially, Ziegler-Nicholas (Z-N) proposed new guidelines for controller tuning. This method completely uses the trial-and-error method which is not considered for the open loop control process.

The output of PI controller is,

$$u(t) = K_P e(t) + K_i \int_0^t e(t)dt \tag{24}$$

4.1. Control of solar photovoltaic system

Two PV panels 100 V each is used as the PV input to the proposed converter. The MZSC boosts the 200 V to 600 V. Figure 6 presents the control system for the solar photovoltaic system. The HDL method is used for accurately predicting the power from solar and wind systems. This predicted power is compared with the actual power in the comparator and the error obtained is fed as input to the PI controller followed by a PWM generator to produce pulse to the modified Z source converter. Thus 600 V DC is produced as the output from the proposed converter.

4.2. Control of WECS

The wind energy conversion system consists of DFIG, turbine blades, Diode bridge Rectifier (DBR) and a boost converter. The DFIG is connected to the wind turbine for harvesting variable AC power from the wind. The speed of the wind ranges from 10 m/s to 12 m/s. The obtained variable AC power is fed to diode bridge rectifier unit and a constant 500 V DC output is obtained from the DBR. This 500 V DC is boosted to 600 V DC using a boost converter. Figure 7 presents the control system of the wind energy conversion system. It is observed that a conventional PI controller is used to provide gating pulses to the switch of a boost converter, to boost the DC voltage from DBR to the required DC-link voltage (600 V)

4.3. Control of bidirectional DC-DC converter

A bidirectional converter is implemented for compensation of power during an increase in the use of loads. Whenever the power produced from the renewable sources is excess, the bidirectional converter operates as a buck converter and stores the excess power in battery and when there is unavailability of power from renewable sources the battery bank supplies power to grid. During this operation, the converter acts as a boost converter. Figure 8 presents the control system of the bidirectional DC-DC converter.

4.4. Control of voltage source inverter

The inverter plays a prominent role in the proposed system. The DC output fed from the z-source network is fed to the voltage source inverter circuit. The

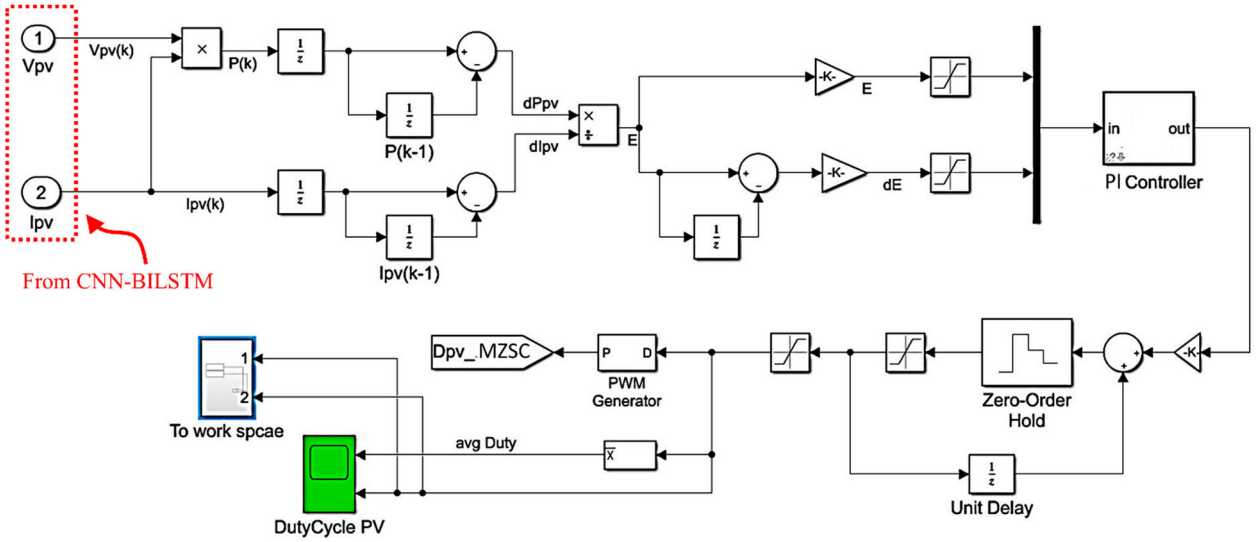

Figure 6. Duty cycle generation for the MZSC.

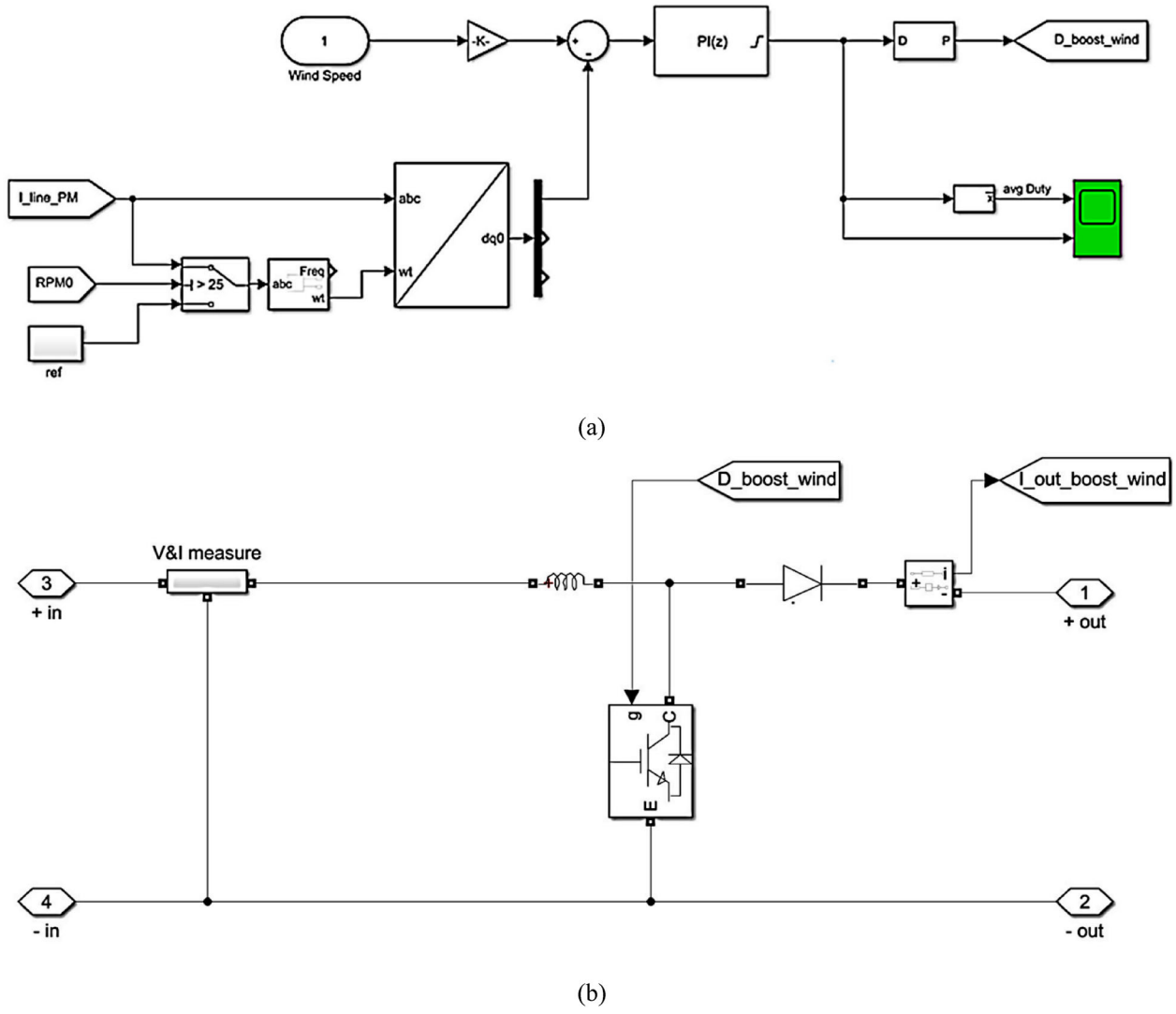

Figure 7. Control system of (a) WECS (b) boost converter.

voltage source inverter consists of six IGBT switches ($S_1, S_2, S_3, S_{4'}, S_{5'}, S_{6'}$)

The pulses to the inverter switches are obtained using the SVPWM [27] method. SVPWM method is depicted in Figure 9, where the six vectors $V1$–$V6$ partition the corresponding space vector into six segments.

Let us consider a sector $V1$ having a coordinate value of (1,0,0). The coordinate "1" describes the triggering

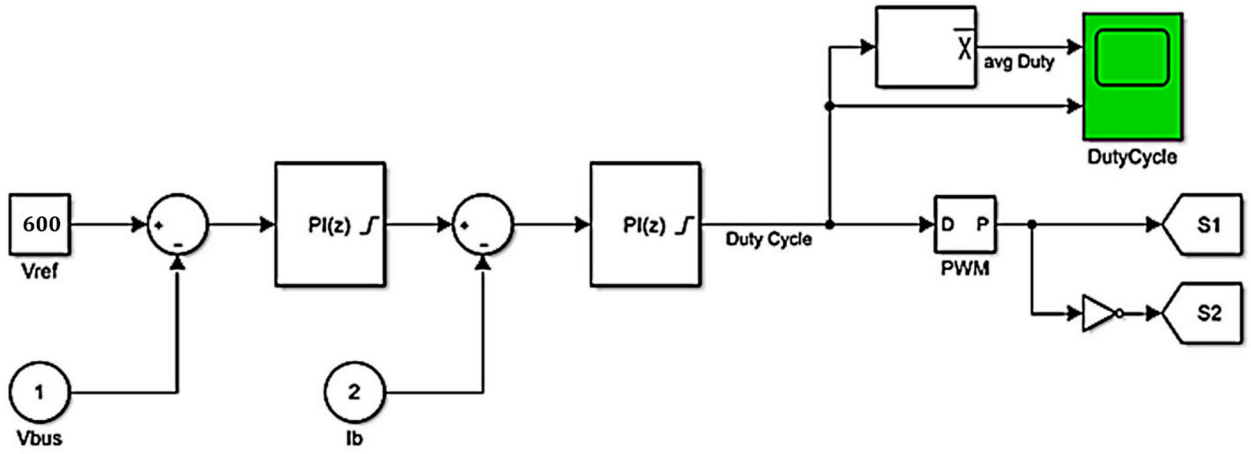

Figure 8. Control system of the DC-DC bidirectional converter.

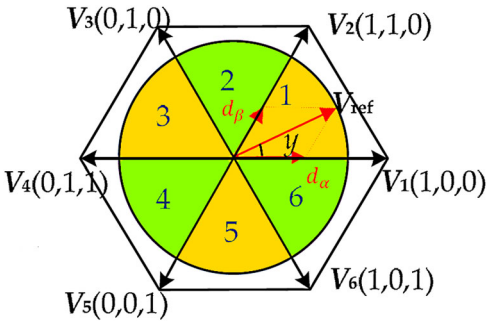

Figure 9. SVPWM for Inverter switches.

of the switch S_1 for the phase a and the other two coordinates "0, 0" denote the triggering of the switches S_5, S_6 for the other two phases b and c respectively. The ranges of current and voltage reference vectors used for controlling the rectifier and inverter circuit is $\left(-\frac{\pi}{6}, \frac{\pi}{6}\right)$ and $\left(0, \frac{\pi}{3}\right)$. The duty cycle required to operate the switches corresponding to the active state $(V1, V2)$ and the zeroth state $(Vo, V7)$ is presented in Equation (25). Table 1 presents the switching sequence of the VSI.

$$\begin{cases} \delta_\alpha = \dfrac{\sqrt{3}U_{\text{nef}}}{u_{\text{dc}}} \sin\left[\dfrac{\pi}{3} - y + \dfrac{\pi}{3}(k_{\text{out}} - 1)\right] \\ \delta_\beta = \dfrac{\sqrt{3}U_{\text{ref}}}{u_{\text{dc}}} \sin\left[y - \dfrac{\pi}{3}(k_{\text{out}} - 1)\right] \\ \delta_0 = 1 - \delta_\alpha - \delta_\beta \end{cases} \tag{25}$$

4.5. Closed loop controller for the proposed grid connected system

In the closed-loop control systems, the ANN controller [28] is used. The ultimate goal of the proposed controller is to pump clear sinusoidal current to the grid even when there is distortion in the grid voltage or operation of a nonlinear load or any voltage imbalance. Due to its durability, easy operation and reliability, the ANN controller is used for control loop operation in GCPVS. The output of the inverter should be sinusoidal for appropriate synchronization of grid. Therefore, it is evident that the input provided to the inverter for the hybrid system should have lower THD, and faster dynamic response. To gain maximum power from the hybrid system and inject sinusoidal current into the

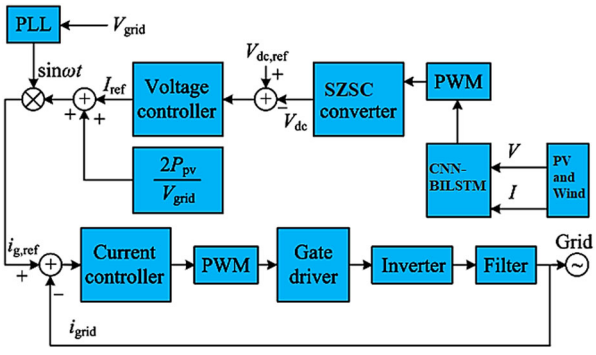

Figure 10. Closed loop control system for the hybrid grid connected system.

Table 1. Switching strategy for the inverter switches.

Vector	S_1	S_2	S_3	S_4	S_5	S_6	U_{AB}	U_{BC}	U_{CA}	*Vector state*
$V0 = \{000\}$	✗	✗	✗	✓	✓	✓	0	0	0	*Zero*
$V1 = \{100\}$	✓	✗	✗	✗	✓	✓	$+U_{dc}$	0	$-U_{dc}$	*Active*
$V2 = \{110\}$	✓	✓	✗	✗	✗	✓	0	$+U_{dc}$	$-U_{dc}$	*Active*
$V3 = \{010\}$	✗	✓	✗	✓	✗	✓	$-U_{dc}$	$+U_{dc}$	0	*Active*
$V4 = \{011\}$	✗	✓	✓	✓	✗	✗	$-U_{dc}$	0	$+U_{dc}$	*Active*
$V5 = \{001\}$	✗	✗	✓	✓	✓	✗	0	$-U_{dc}$	$+U_{dc}$	*Active*
$V6 = \{101\}$	✓	✗	✓	✗	✓	✗	$+U_{dc}$	$-U_{dc}$	0	*Active*
$V7 = \{111\}$	✓	✓	✓	✗	✗	✗	0	0	0	*Zero*

grid, an interface between the hybrid system and the grid must be used.

Figure 10 presents the closed-loop control system of the proposed GCPVS. The voltage control loop controls the DC link voltages from the hybrid system and the Current loop controls the inverter current. Power quality standards must be established throughout the grid-connected system to meet the grid interconnection.

5. Results and discussion

5.1. Simulation results

The proposed system is tested with the developed hybrid system and Hybrid DL method in MATLAB/SIMULINK platform. Table 2 presents the parameters used for designing the proposed system. Table 3 presents the parameters used for designing the hybrid DL method. A combinational deep learning approach is developed based on the CNN and Bi-LSTM, which incorporates short-term solar and wind power forecasting. Convolutional layers have a kernel size of 64 and 128. There are 64 and 128 neurones beneath the surface of the hidden layers of BiLSTM [29].

To obtain the expected wind and solar power output, there is a single dense layer with 512 neurones.

Table 2. Parameters of the proposed hybrid system.

Load sizing	DC Bus Voltage	600 Vdc
	Load Power Required	1 kW
Battery sizing	Batteries capacity	102 Ah
	Battery Voltage	96 Vdc
	Batteries capacity	9.8 kWh
	Batteries strings (parallel)	1
	Batteries per string (series)	4
PV array sizing	PV module	Soltech 1STH − 215 − P
	Max power per module	100 W
	Max current	7.35 A
	Max voltage	65 V
	Parallel Strings	6
	Series Modules per string	3
DFIG	Rated Power	500W
	Rated Speed	360 RPM

Table 3. Parameters of the CNN-BiLSTM.

Suggested model		Design parameters	
CNN - BiLSTM		Units1	Units = 64;
		Units2	Units = 128;
	Drop out	Drop out = 0.2	
	CNN	Convolution (PV)	Filter = 64
			Kernel size = 3
			Stride = 1
		Max - pooling (PV)	Kernel size = 2
			Stride = 1
		Convolution (Wind)	Filter = 128
			Kernel size = 3
			Stride = 1
		Max - pooling (Wind)	Kernel size = 2
			Stride = 1
	Drop out	Drop out = 0.2	
	Fully connected	Neurons = 512	
Epoch = 140, Batch size = 200; Optimizer = Adam′; Learning rate = 0.002.			

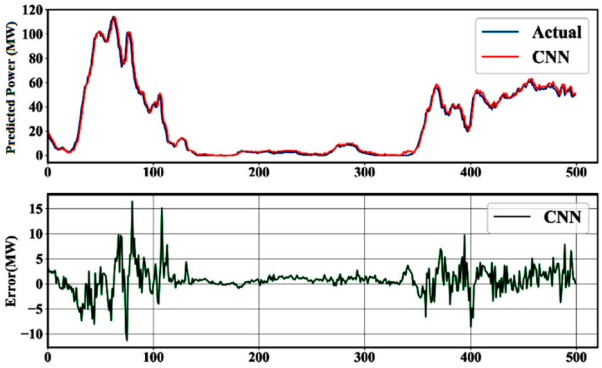

Figure 11. Simulation output of actual power with the predicted power using CNN method.

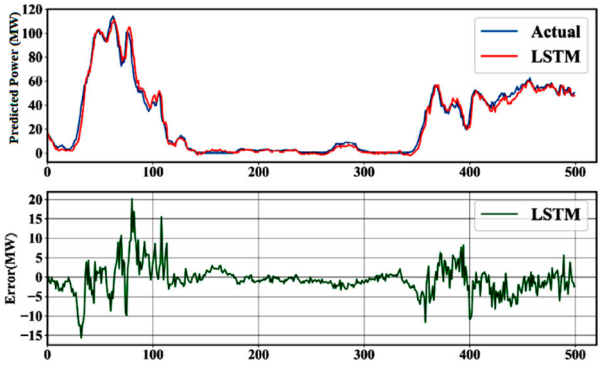

Figure 12. Simulation output of actual power with the predicted power using LSTM method.

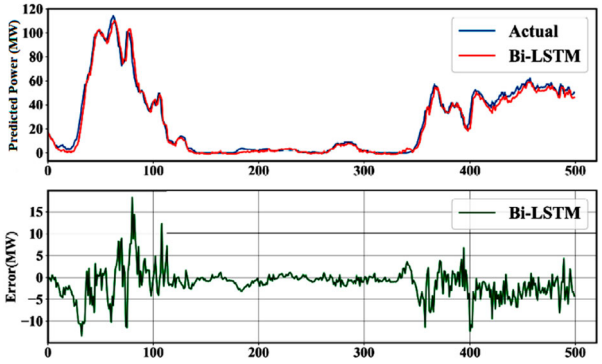

Figure 13. Simulation output of actual power with the predicted power using Bi-LSTM method.

Dropout layers are used to mitigate the model's prediction error, and they are applied to both the framework and the dropout rate is considered as 0.2 and 0.1. The learning rate is 0.001, and Adam optimizer is used. The proposed method is compared with three conventional DL methods to check the performance of the proposed method. All DL models are derived from the same set of data. Figures 11–14 presents the simulation results of the CNN, LSTM, Bi-LSTM and the proposed hybrid DL model.

Table 4 presents the performance of various DL methods using error parameters under varying Solar

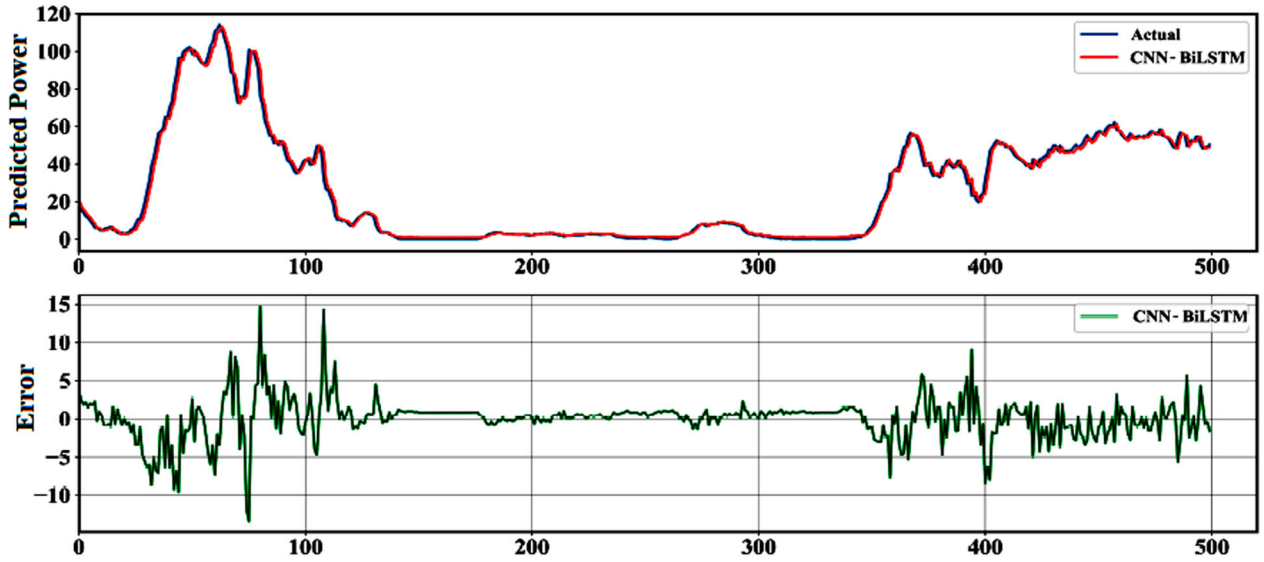

Figure 14. Simulation output of actual power with the predicted power using CNN-BiLSTM method.

Table 4. Performance of various DL methods using error parameters under varying solar data.

Error parameters	CNN	LSTM	Bi - LSTM	CNN - BiLSTM
MSE	0.1030	0.1045	0.0911	0.0884
MAE	0.0517	0.0455	0.0311	0.0219
r^2	0.7256897	0.8986598	0.7136045	0.9931256
Skew	0.7127638	0.8125689	0.9589671	0.9999235
Kurtosis	−0.512698	−0.458634	−0.315962	−0.253674

Table 5. Performance of various DL methods using error parameters under varying wind data.

Error parameters	CNN	LSTM	Bi - LSTM	CNN - BiLSTM
MSE	6.3759	5.3143	6.1136	2.1432
MAE	2.6874	2.1156	1.3955	1.0125
r^2	0.9918	0.9865	0.9877	0.9920
Skew	0.4352	0.6168	0.8756	0.9998
Kurtosis	−0.711563	−0.636578	−0.575632	−0.246351

data and Table 5 presents the performance of various DL methods using error parameters under varying wind data. Figure 15 presents the graphical illustration of performance of DL methods used in predicting the solar output power with their respective errors.

Figure 16 presents the graphical illustration of performance of DL methods used in predicting the wind output power with their respective errors. These investigations from the findings provide strong evidence to suggest that the suggested hybrid DL model is the most effective model which has a lower MSE value of 0.0884, lower MAE value of 0.0219, has the highest skew and r^2 value of 0.9999235, 0.9931256 and a lower kurtosis value of −0.253674 for solar data and the same DL method gives lower MSE value of 2.1432, lower MAE value of 1.0125, has the highest skew and r^2 value of 0.9920, 0.9998 and a lower kurtosis value of −0.246351 for wind data. From the charts in Figures 15 and 16, it can be observed that the curve of the CNN-BiLSTM model is most closely matched to the real solar and wind power output curve, with a small forecast error. During rapidly-changing wind and solar power, this model has the smallest prediction error. However, the computational performance of CNN-BiLSTM is the slowest, with a mean processing duration of 0.4752 s. As well, CNN's processing duration is the fastest out of all the models, with an estimated duration of 0.0741 s.

Figure 17 presents the output waveforms of the solar PV system. The input radiation received by the PV panels ranges from 800 w/m^2 to 1000 w/m^2. The DC voltage obtained from the PV panel is 200 V and the output power obtained from the PV system is about 1 Kwp (10 panels of 100 watts).

Figure 18 presents the waveforms of the wind energy conversion system. From Figure 18 it is observed that the wind speed in the wind energy conversion system is varied from 10 m/s to 12 m/s. The voltage obtained by the DFIG (double fed induction generator) is 500 V and the DC voltage obtained at the output of the PWM rectifier is 600 V.

Figure 19 presents the output waveforms of the proposed switched Z-source converter. The values of L_1, L_2 and C_1, C_2 can be determined by using the formulas presented in Equation (26). From Figure 19 it is observed that the input voltage to the proposed MSZSC is 200 V. When the duty cycle is varied and fixed to a value of 0.33, the voltage found across the capacitors C_1 and C_2 are 300 V each and the output of the MSZSC is 600 V. When the duty cycle is adjusted to 0.42, the voltage of capacitors C_1, C_2 changes to 350 V, 400 V and the output of MSZSC is 750 V.

$$\left.\begin{aligned} L_1, L_2 &= \frac{2V_{pv}D(1-D)}{x_L.I_o f_{sw}} \\ C_1, C_2 &= \frac{I_o D}{x_C.f_{sw}V_i(1-2D)} \end{aligned}\right\} \quad (26)$$

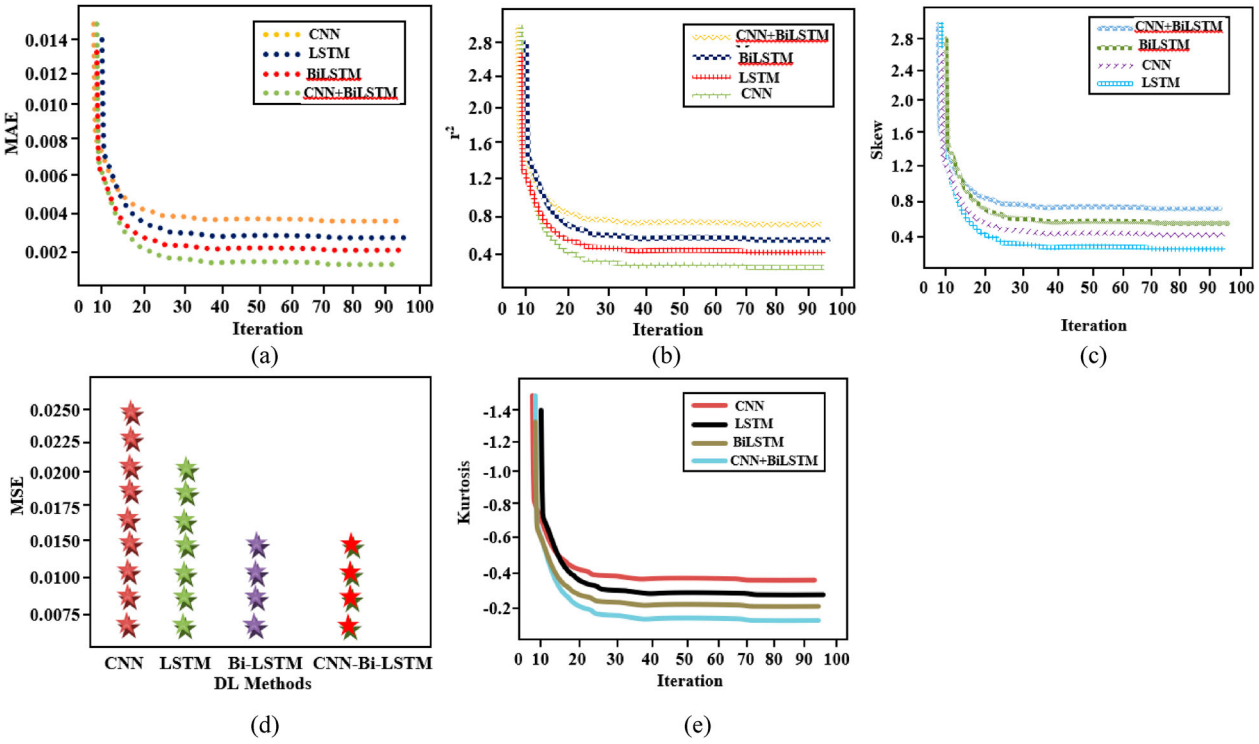

Figure 15. Comparison of (a) MAE vs iteration (b) r^2 vs iteration (c) Skew vs iteration (d) MSE vs DL methods (e) kurtosis vs iteration errors in predicting the solar output power.

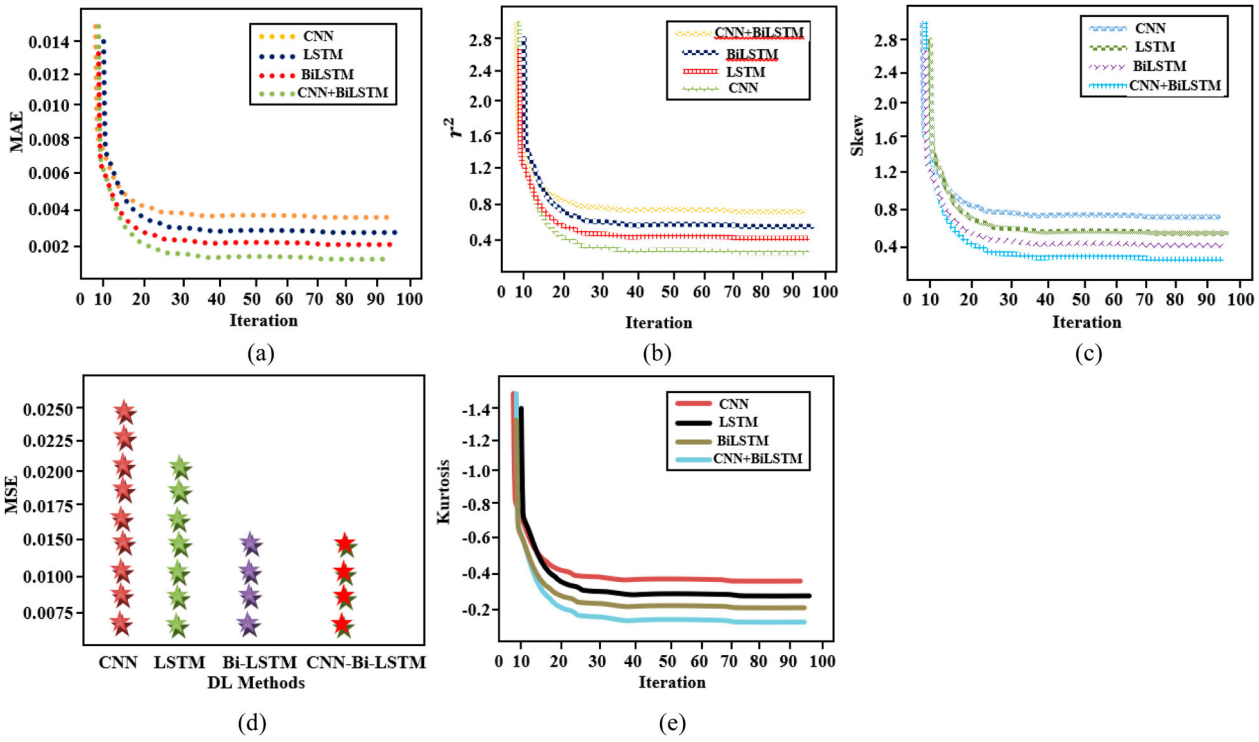

Figure 16. Comparison of (a) MAE vs iteration (b) r^2 vs iteration (c) skew vs iteration (d) MSE vs DL methods (e) kurtosis vs iteration errors in predicting the wind output power.

The terminal voltage of the battery pack and the PCC is shown in Figure 20. The SOC is efficiently regulated with the help of the bidirectional controller, and energy is observed to be transferring from the batteries continuously. The SOC is generally considered to be 70%. The SOC may vary based on changes in the output of the MSZSC and PWM rectifier. A steady voltage is maintained at the PCC by the control system for a time period of 0.2 s, and the battery returns to its original voltage. As a result, the controller demonstrates remarkable tracking and learning capabilities. According to this theory, an effective energy management

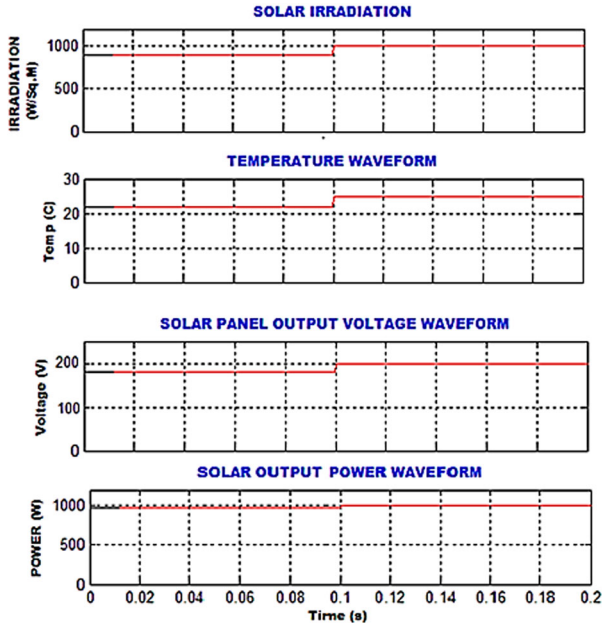

Figure 17. Simulation output of solar PV system.

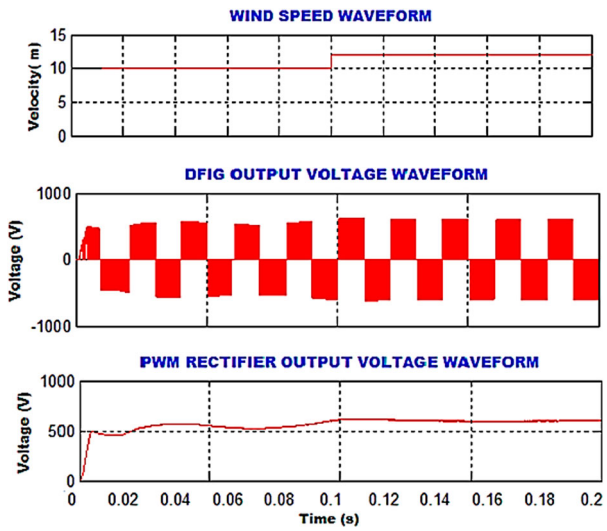

Figure 18. Simulation output of wind energy conversion system.

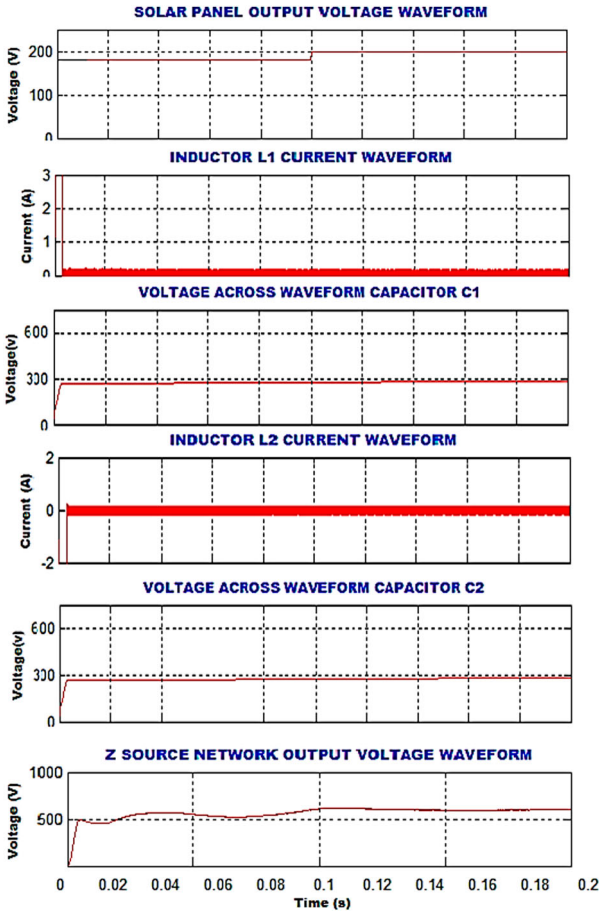

Figure 19. Simulation output of the proposed MSZSC.

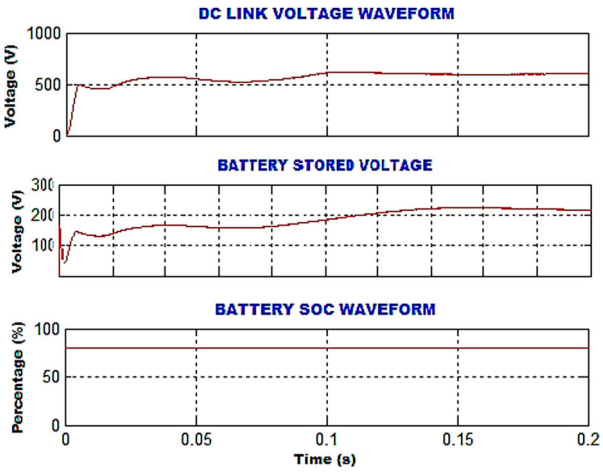

Figure 20. Simulation output of DC-link and Battery voltage.

system has been developed, allowing a constant PCC voltage to be retained even when the power source changes. ANN controller with SVPWM is utilized to regulate the voltage of the inverter, while closed-loop control system based on PI controller is implemented for MSZSC to maintain a constant dc link voltage of 600 V at PCC. Figure 21 presents the pulse generation to the VSI using SVPWM. Figure 22 presents the output waveforms of the grid-connected system. Figure 23 presents the grid voltage, grid current and THD of grid current using the PI controller. Figure 24 presents the grid voltage, grid current and THD of grid current with the ANN controller. It is observed that the THD of the grid current obtained using conventional PI controller has more harmonics, especially the lower order harmonics which are more dominant than the fundamental and give almost 6% of THD which is greater than the IEEE 519 standard value, whereas the THD of the grid current obtained using ANN controller is only 2.47%.

5.2. Hardware results

The solar and wind energy system including battery storage system is built in the laboratory. Figure 25 presents the prototype of the proposed system. The

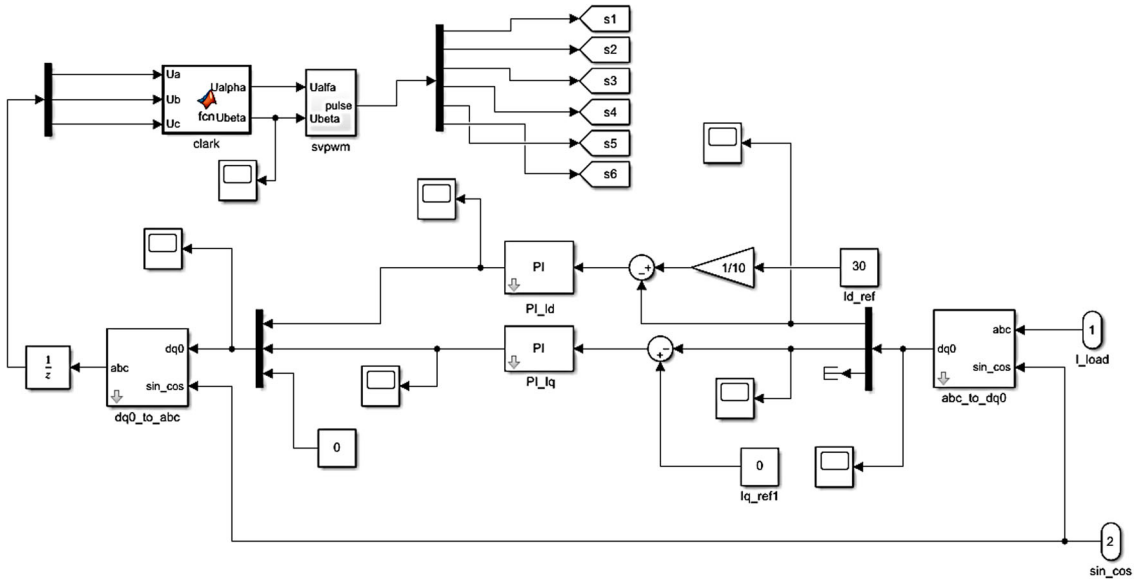

Figure 21. Pulse generation using SVPWM method.

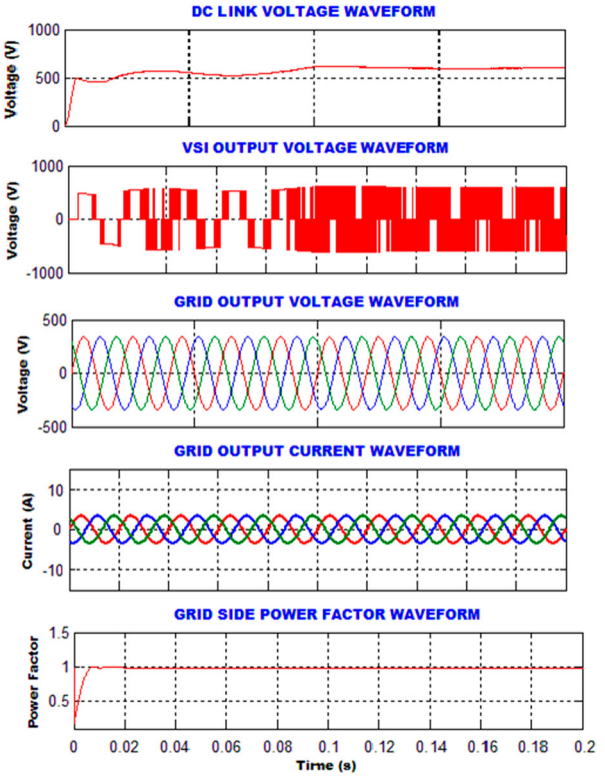

Figure 22. Simulation output of GCHS.

voltage at the PCC is used as a reference voltage by the controller, and the control signal is fed back via inverter and appropriate filters. To operate the inverter with an independent gate driver, the ANN controller needs onboard PWM circuits. Using an EM relay and input–output contact pins, the power contactor is operated. FPGA controller (dsPIC3050) automates the entire system. Figure 26 presents the experimental output waveforms of the PV voltage, current through the

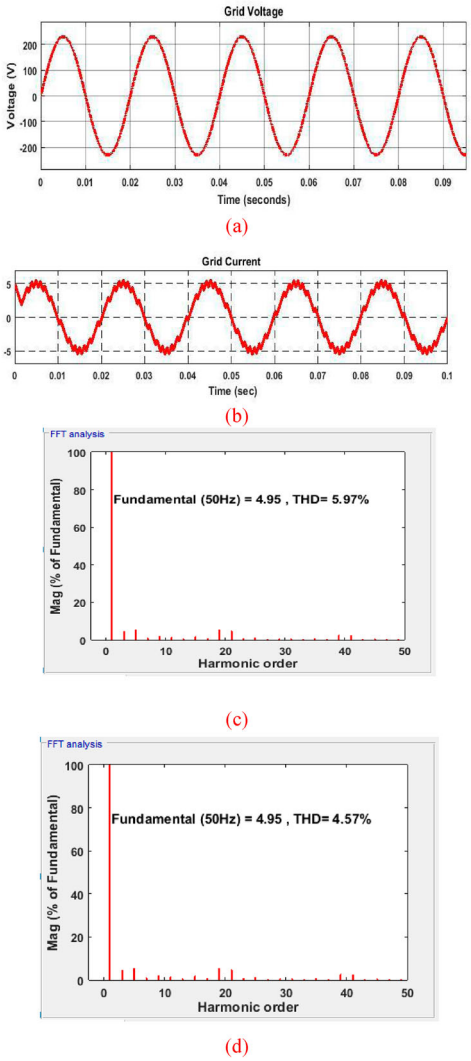

Figure 23. Simulation Result of (a) Grid voltage (b) Grid current (c) FFT analysis of Grid current with PI controller (d) FFT analysis of Grid current with Fuzzy controller.

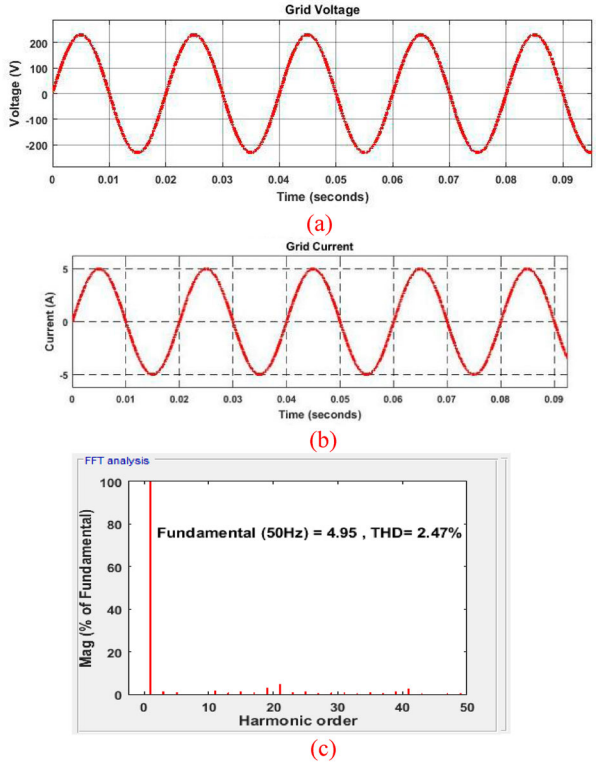

Figure 24. (a) grid voltage (b) grid current (c) FFT analysis of grid current using ANN controller.

inductors L_1, L_2 voltage across the capacitors C_1, C_2, output voltage of the proposed MSZSC, output voltage of the DFIG, rectifier output voltage.

Figure 27 presents the experimental output of battery voltage, DC-link voltage, inverter voltage, injected grid current from the inverter and the total harmonic distortion (THD) of the grid current. From Figure 27(d) it is observed that the grid current is sinusoidal in nature and is in phase with the grid voltage and maintains a unity power factor. Moreover, from Figure 27(e) it is observed that the THD of the grid current is approximately equal to 2% which is very low and is within the IEEE-519 standard. The use of ANN controller with space vector pulse width modulation method gives a THD of 2.2%. Table 6 presents the performance comparison of different controllers for the proposed MSZSC. From Table 6 it is observed that the PI controller performs well when compared with other controllers. There is a direct correlation between duty ratio and voltage transfer ratio as shown in Figure 28, which compares the voltage gain of various DC-DC converters. When using a 40% duty cycle, the voltage gain of MSZSC reaches a maximum of 10, while the gains for the Landsman and LUO converters are only about 6 and 3.5 at that point. The switching losses fall drastically as the duty cycle reduces, but the system's total performance stays the same.

Table 7 presents the comparison of THD of the grid current with different controllers using the SVPWM modulation method. From the table, it is evident that

Figure 25. (a) prototype of the proposed system (b) wind and solar PV module (c) Wind generator set.

the proposed system performs well using ANN controller and SVPWM method. Figure 29 presents the graphical comparison of the proposed system with different controllers. From Figure 29 it is evident that the performance of the system by implementing the ANN

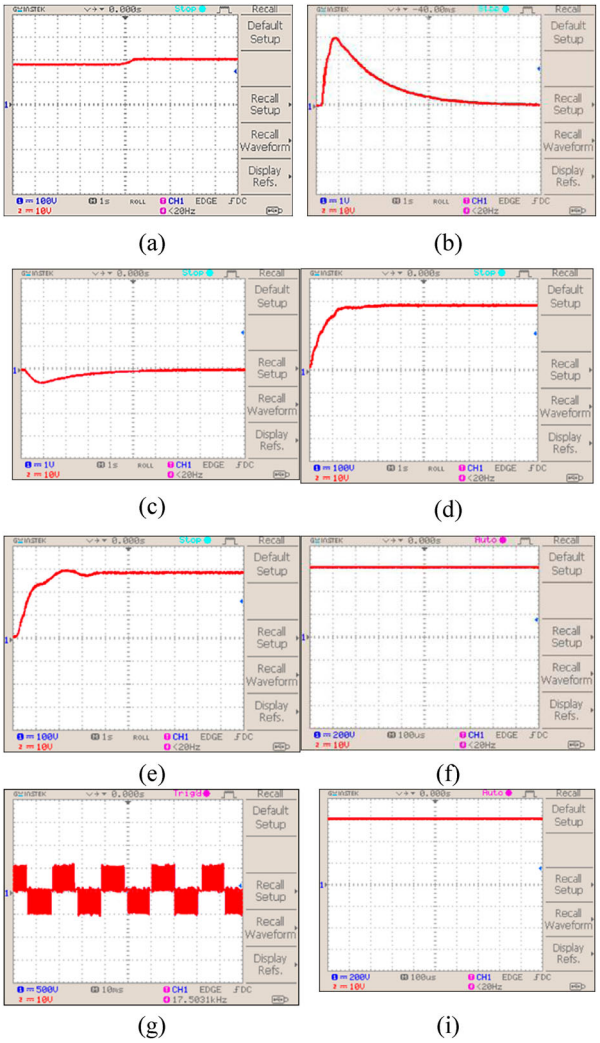

Figure 26. Experimental output (a) PV voltage (b) Inductor current L_1 (c) Inductor current L_2 (d) capacitor voltage C_1 (e) capacitor voltage C_2 (f) Voltage of MSZSC (g) voltage of DFIG (i) Rectifier voltage.

Table 6. Comparative analysis of PI controller and fuzzy controller in terms of risetime, peak time, settling time and steady state error.

Controller	K_p	K_I	(t_r)	(t_p)	(t_s)	ess
P&O Method	0.1812	7.1653	0.2395	0.5728	0.6321	0.67
Fuzzy controller	0.2986	11.1251	0.1296	0.2988	0.4522	0.21
PI controller	0.3238	30.1512	0.041	0.1053	0.1102	0.13

Table 7. THD Comparison of grid current using different controllers.

Method	PI Sim	Fuzzy Sim	ANN H/W	
SVPWM	5.97%	4.57%	2.47%	2.21%

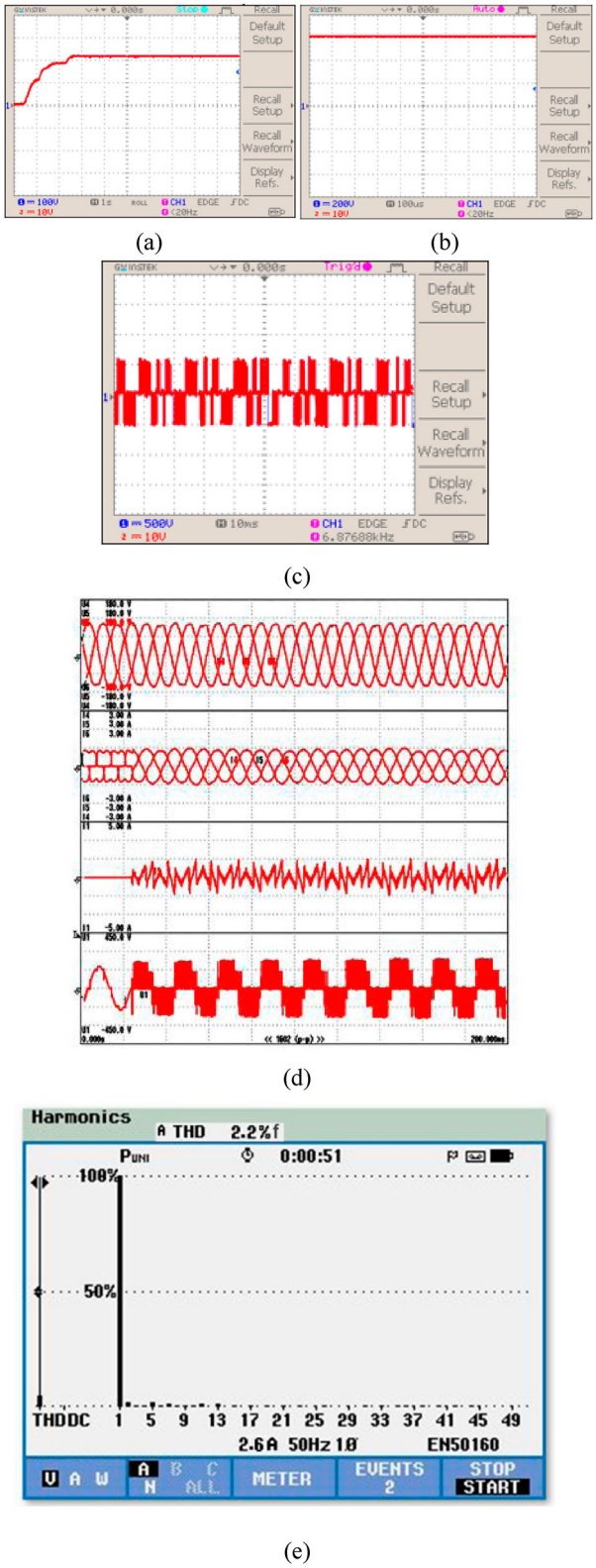

Figure 27. Experimental output (a) battery voltage (b) DC-link voltage (c) inverter voltage (d) Injected grid current (e) THD of the grid current.

controller with the SVPWM method outperforms well in both simulation as well as prototype.

Figure 30 presents the comparison of the grid current THD of the proposed system with other existing works [30–33]. From Figure 30 it is observed that the proposed system uses the ANN controller to inject harmonic less current into the grid when compared with other existing work. From the above analysis, it is concluded that the ANN controller produces a harmonic less grid current and maintains the grid current within the IEEE-519 standard. But the Fuzzy controller also works effectively and produces an optimum harmonic content of (4.57% in simulation). The only drawback of

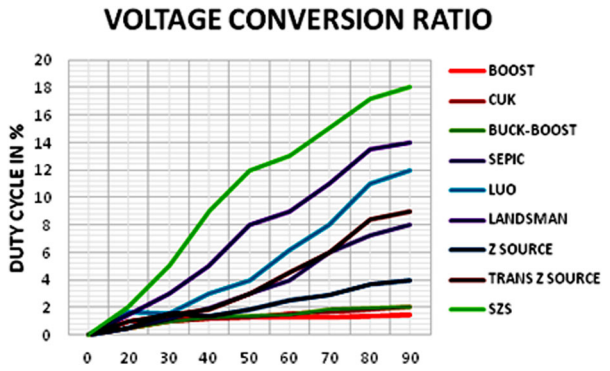

Figure 28. Comparison of voltage gain ratio of different DC-DC converters.

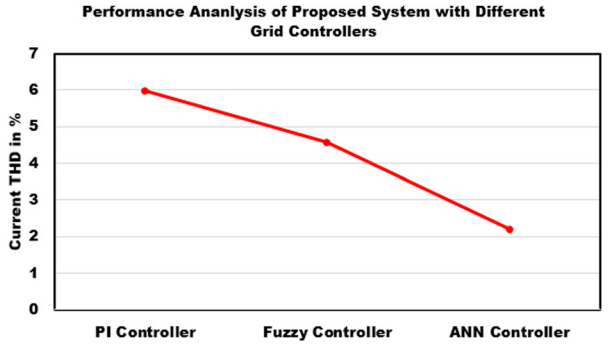

Figure 29. Comparison of THD of Grid current using various controllers.

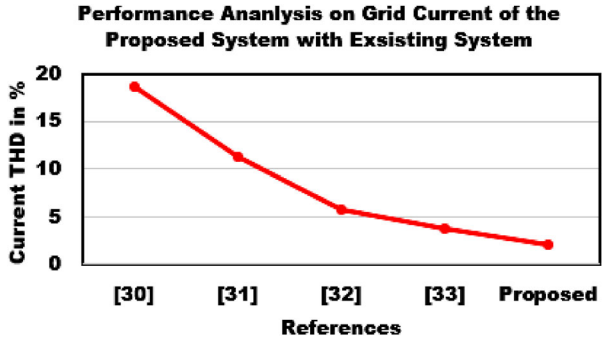

Figure 30. Comparison of proposed work with existing similar work.

a fuzzy controller is a slower response to any change in the output of the system (grid voltage).

6. Conclusion

This paper mainly focuses on the implementation of the hybrid deep learning method for accurate forecasting of the wind and solar power. The actual power obtained from the renewable energy sources is compared with the predicted power and the error is being processed in a PI controller to switch the modified Z source converter for the PV system and the conventional boost converter for the wind power system. A 600 V constant DC voltage is obtained from the MZSC as well as the conventional boost converter which is then fed to the VSI. The computational performance of CNN-BiLSTM is slightly slower, with a mean processing duration of 0.4752 s when compared with the CNN's processing duration of 0.0741 s. But the accuracy in prediction is high in HDL method compared to DL method. In order to maintain a constant power supply, a battery storage system is also used to balance energy between the source and the grid. Predicting solar power at its peak, tracking the rectified output of wind turbine to match peak wind power, and utilizing effective battery energy management all work together to provide uninterruptible power supply to the grid. The developed system provides power similar to the distributed system's optimal levels even under poor climatic conditions, and also supplies continuous power even though the energy from the PV and wind sources is zero. The proposed grid-connected system is tested using a conventional PI controller, Fuzzy controller and ANN controller. The suggested control strategy can individually control the renewable energy sources. The grid current's THD content is kept far below the IEEE519 standard. The conventional PI controller gives a THD content of 5.97%, the fuzzy controller gives a THD content of 4.57% and the ANN controller gives a THD content of 2.21%. The use of ANN controller with the SVPWM method outperforms well when compared with other conventional controllers. The proposed work injects harmonic less current to the grid while compared with the other existing work.

Disclosure statement

No potential conflict of interest was reported by the author(s).

ORCID

T. Anu Shalini http://orcid.org/0000-0001-7044-2208
B. Sri Revathi http://orcid.org/0000-0001-5608-5574

References

[1] Vanaja DS, Stonier AA, Mani G, et al. Investigation and validation of solar photovoltaic-fed modular multilevel inverter for marine water-pumping applications. Electr Eng. 2022;104(3):1163–1178.
[2] Albert JR, Vanaja DS. "Solar energy assessment in various regions of Indian Sub-continent." . Solar Cells Theory, Materials and Recent Advances. 2020.
[3] Shunmugham Vanaja D, Albert JR, Stonier AA. An experimental investigation on solar PV fed modular STATCOM in WECS using intelligent controller. Int Trans Electr Energy Syst. 2021;31(5):e12845.
[4] Jebli I, Belouadha FZ, Kabbaj MI, et al. Prediction of solar energy guided by Pearson correlation using machine learning. Energy. 2021;224:120109.
[5] Park S, Kim Y, Ferrier NJ, et al. Prediction of solar irradiance and photovoltaic solar energy product based on cloud coverage estimation using machine learning methods. Atmosphere. 2021;12(3):395.
[6] Li LL, Cen ZY, Tseng ML, et al. Improving short-term wind power prediction using hybrid improved cuckoo

search arithmetic – support vector regression machine. J Cleaner Prod. 2021;279:123739.
[7] Huang D, Wang S, Liu Z. A systematic review of prediction methods for emergency management. Int J Disaster Risk Reduct. 2021;62:102412.
[8] Upadhyay KG, Choudhary AK, Tripathi MM. Short-term wind speed forecasting using feed-forward back-propagation neural network. Int J Eng Sci Technol. 2011;3(5):107–112.
[9] Zhu X, Genton MG. Short-term wind speed forecasting for power system operations. Int Stat Rev. 2012;80(1):2–23.
[10] Tung TM, Yaseen ZM. Deep learning for prediction of water quality index classification: tropical catchment environmental assessment. Nat Resour Res. 2021;30(6):4235–4254.
[11] Rai A, Shrivastava A, Jana KC. A CNN-BiLSTM based deep learning model for mid-term solar radiation prediction. Int Trans Electr Energy Syst. 2021;31(9):e12664.
[12] Meng F, Zou Q, Zhang Z, et al. An intelligent hybrid wavelet-adversarial deep model for accurate prediction of solar power generation. Energy Rep. 2021;7:2155–2164.
[13] Palanivel V, Govindasamy K, Arunachalam GK. Optimization and prediction of pulsating heat pipe compound parabolic solar collector performances by hybrid deep belief network based bald eagle search optimizer. Environ Prog Sustain Energy. 2021;41(2):e13740.
[14] Peng T, Zhang C, Zhou J, et al. An integrated framework of bi-directional long-short term memory (BiLSTM) based on sine cosine algorithm for hourly solar radiation forecasting. Energy. 2021;221:119887.
[15] Huang S, Li P, Yang M, et al. A control strategy based on deep reinforcement learning under the combined wind-solar storage system. IEEE Trans Ind Appl. 2021;57(6):6547–6558.
[16] Al-Hajj R, Assi A, Fouad M, et al. A hybrid LSTM-based genetic programming approach for short-term prediction of global solar radiation using weather data. Processes. 2021;9(7):1187.
[17] Vakitbilir N, Hilal A, Direkoğlu C. Hybrid deep learning models for multivariate forecasting of global horizontal irradiation. Neural Comput Appl. 2022;34(10):8005–8026.
[18] Hossain MA, Chakrabortty RK, Elsawah S, et al. Very short-term forecasting of wind power generation using hybrid deep learning model. J Cleaner Prod. 2021;296:126564.
[19] Hossain MA, Chakrabortty RK, Elsawah S, et al. Predicting wind power generation using hybrid deep learning with optimization. IEEE Trans Appl Supercond. 2021;31(8):1–5. Art no. 0601305. doi:10.1109/TASC.2021.3091116
[20] Li G, Xie S, Wang B, et al. Photovoltaic power forecasting with a hybrid deep learning approach. IEEE Access. 2020;8:175871–175880. doi:10.1109/ACCESS.2020.3025860
[21] Sanjari MJ, Gooi HB, Nair NC. Power generation forecast of hybrid PV–wind system. IEEE Trans Sustain Energy. 2020;11(2):703–712. doi:10.1109/TSTE.2019.2903900
[22] Kothona D, Panapakidis IP, Christoforidis GC. A novel hybrid ensemble LSTM-FFNN forecasting model for very short-term and short-term PV generation forecasting. IET Renew Power Gener. 2022;16(1):3–18.
[23] Aly HH. A hybrid optimized model of adaptive neuro-fuzzy inference system, recurrent Kalman filter and neuro-wavelet for wind power forecasting driven by DFIG. Energy. 2022;239:122367.
[24] Zafar MH, Khan NM, Mansoor M, et al. Adaptive ML-based technique for renewable energy system power forecasting in hybrid PV-wind farms power conversion systems. Energy Convers Manage. 2022;258:115564.
[25] Shunmugham Vanaja D, Stonier AA. A novel PV fed asymmetric multilevel inverter with reduced THD for a grid-connected system. Int Trans Electr Energy Syst. 2020;30(4):e12267.
[26] Garud KS, Jayaraj S, Lee MY. A review on modeling of solar photovoltaic systems using artificial neural networks, fuzzy logic, genetic algorithm and hybrid models. Int J Energy Res. 2021;45(1):6–35.
[27] Lewicki A, Odeh CI, Kondratenko D, et al. Hybridized space-vector pulse width modulation for multiphase two-level voltage source inverter. IEEE Trans Power Electron. 2022;37(7):7663–7674.
[28] Shunmugham Vanaja D, Stonier AA, Moghassemi A. A novel control topology for grid-integration with modular multilevel inverter. Int Trans Electr Energy Syst. 2021;31(12):e13135.
[29] Li C, Zhang Y, Zhao G, et al. Hourly solar irradiance prediction using deep BiLSTM network. Earth Sci Inf. 2021;14(1):299–309.
[30] Han Y, Chen H, Li Z, et al. Stability analysis for the grid-connected single-phase asymmetrical cascaded multilevel inverter with SRF-PI current control under weak grid conditions. IEEE Trans Power Electron. 2019;34(3):2052–2069.
[31] Bihari S, Sadhu P. Design analysis of high level inverter with EANFIS controller for grid connected PV system. Analog Integr Circuits Signal Process. 2020;103(3):411–424.
[32] Salem WAA, Ibrahim WG, Abdelsadek AM, et al. Grid connected photovoltaic system impression on power quality of low voltage distribution system. Cogent Eng. 2022;9(1):2044576.
[33] Kanouni B, Badoud Abd E, Mekhilef S. A multi-objective model predictive current control with two-step horizon for double-stage grid-connected inverter PEMFC system. Int J Hydrogen Energy. 2022;47(4):2685–2707.